Indian Journal of Chemistry
Vol. 57A, February 2018, pp. 143-149

Theoretical study of ^{11}B NMR chemical shifts of prototypical boranes: The case of *closo*-$[B_{12}H_{12}]^{2-}$, *nest*-$B_{11}H_{15}$, and *arachno*-$B_{10}H_{16}$

A Morales-Bayuelo[a, b], J M Catalán Lavín[c] & R Ramírez-Tagle[c, *]

[a]Centro de Investigación de Procesos del Tecnológico Comfenalco. Fundación Universitaria Tecnológico Comfenalco, Cartagena de Indias, Colombia
[b]Grupo de investigaciones básicas y clínicas de la universidad del Sinú, Cartagena de Indias, Colombia
[c]Facultad de Ingenieria Ciencia y Tecnologia, Universidad Bernardo O´Higgins, Santiago, Chile
Email: rramirez@ubo.cl

Received 31 July 2017; re-revised and accepted 31 January 2018

The structural and electronic dependence of the ^{11}B chemical shifts for a series of borane structures, namely, *closo*-$[B_{12}H_{12}]^{2-}$, *nest*-$[B_{11}H_{15}]$, and *arachno*-$[B_{10}H_{16}]$ are investigated using density functional theory calculations. Three types of environments are identified for the borane systems, in increasing order of chemical shielding as: B-H < B-H-B < B-B-B. The obtained chemical shifts are in good agreement with the available experimental results and reflect the extent of heterogeneity of the electronic environments present in these chemical systems in terms of symmetry and the number of boron cores. In addition, results of molecular quantum similarity studies using similarity descriptors such as overlap and coulomb indices and Euclidean distances are also reported.

Keywords: Theoretical chemistry, Borane clusters, Superatoms, NMR spectroscopy, Quantum similarity

Borane cages are well understood in terms of the popular Wade's skeletal-electron rule, which accounts for their favorable stability and bonding[1,2]. Structurally, boranes are three-dimensional, skeleton polyhedral clusters with closed or open faces (e.g., *closo*, *nest*, *arachno*, and *hypo*)[3]. Boranes provide a link to the structural features of condensed fragments of metal-based networks, and their molecular structures, both linear and cyclical, give insight of organic and inorganic π-bonding systems. Ken Wade developed a method for predicting borane cluster forms that can be used for a wide range of substituted boranes (such as carboranes, haloboranos, etc.), as well as other types of substituted compounds. These so-called Wade's rules are used to characterize the shape of borane clusters by calculating the total number of skeletal electron pairs (SEP) available for joining the cluster[4]. Using Wade's rules is fundamental to understanding the structural relationship among various boranes[2,5,6]. Thus, for each rule, the "type" of borane under study can be characterized as *closo*, *nest*, or *arachno*.

In the field of inorganic chemistry, X-ray diffraction[7] has contributed to the structural characterization of boranes. Lipscomb deduced the molecular structure of boranes using this technique in the 1950s and developed theories to explain their relationship[3]. Studies conducted by Lipscomb on the three-dimensional structure of borane clusters represent another milestone in the study of these compounds[3,8]. However, despite the wealth of information and the large number of studies conducted over the past century, the chemistry of boron clusters has the same level of development as elements like carbon. For instance, the successful prediction of borane structures can explain the formation of bonds between multiple centers (e.g. 3c-2e)[6].

The present study was performed to contribute to the field of theoretical ^{11}B NMR[8] by examining the chemical environment of representative borane systems. Further, the magnetic response[9] of the nuclei involved in these compounds has been evaluated and compared with the experimental values[4]. This combined computational and theoretical approach to NMR spectroscopy enables determination of the absolute (σ) and relative (δ) chemical shifts of boranes and provides a rationale for these chemical shifts based on the electron density[2,9–11]. Using the Molecular Quantum Similarity (MQS) technique, introduced by Carbó and co-workers[12–16] and which uses similarity indices within the context of density functional theory (DFT), the structural relationship of the investigated boranes was analyzed and developed for each molecular set (i.e., *closo*, *nest*, and *arachno*) to determine the most important parameter that affects their geometries in terms of structural and electronic viewpoints.

Theoretical details

Quantum similarity analyses

Molecular quantum similarity has been used to analyze structural relationships[12–16] and to understand the steric and electronic effects of molecular sets. The mathematic relations to obtain a quantum similarity Z_{AB} between two compounds A and B with electron density $\rho_A(r_1)$ and $\rho_B(r_2)$, respectively, is defined by minimizing the expression for the Euclidean distance as:

$$D_{AB} = \sqrt{\int |\rho_A(r) - \rho_B(r)|^2 \, dr}$$
$$= \sqrt{\int (\rho_A(r_1))^2 dr_1 + \int (\rho_B(r_2))^2 dr_2 - 2\int \rho_A(r_1)\rho_B(r_2) dr_1 dr_2}$$
$$= \sqrt{Z_{AA} + Z_{BB} - 2Z_{AB}} \quad ...(1)$$

Therefore, the Euclidean distance is the square root of the integral of the squared differences between the densities $\rho_A(r_1)$ and $\rho_B(r_2)$. In this context, Z_{AB} represents a measure of similarity between the electronic densities of compounds A and B. Note that Z_{AA} and Z_{BB} are the self-similarity of compounds A and B[17]. The similarity index very often used is the so-called Carbó index[17], which is expressed as follows:

$$I_{AB} = \frac{\int \rho_A(r_1)\rho_B(r_2) dr_1 dr_2}{\sqrt{\int (\rho_A(r_1))^2 dr_1 \int (\rho_B(r_2))^2 dr_2}} = \frac{Z_{AB}(\mathbf{\Omega})}{\sqrt{Z_{AA}(\mathbf{\Omega}) Z_{BB}(\mathbf{\Omega})}} \quad \ldots(2)$$

In Eq. (2), (Ω) represents an operator. A simple way to make a Quantum Similarity Measure (QSM)[16–18] involving two density functions, in the most usual form, is in terms of an integral as (Eq. 3),

$$Z_{AB}(\Omega) = \iint \rho_A(r_1)\Omega(r_1, r_2)\rho_B(r_2) dr_1 dr_2 \quad \ldots(3)$$

where $\rho_A(r_1)$ and $\rho_B(r_2)$ are the density functions of quantum objects A and B, respectively, and $\Omega(r_1,r_2)$ is a positive definite weight operator. When the operator is chosen as the Dirac Delta function (i.e., $\delta(r_1 - r_2)$), we obtain an overlap similarity measure, whereas a Coulomb similarity measure occurs when the operator is chosen as $|r_1 - r_2|^{-1}$. These are the two most popular operators for similarity comparisons between molecules.

Molecular alignment

An optimal molecular alignment is needed to perform the quantum similarity measurements. As the integrals attached to the QSM produce real, positive definite results, the relative position problem can be addressed through a maximal QSM. For an overlap QSM, this situation can be expressed by means of Eq. (4).

$$\max_{T;\phi} Z_{AB}(T;\phi) = \max_{T;\phi} \int \rho_A(r)\rho_B(r|T;\phi) dr \quad \ldots(4)$$

Here, it is implicitly understood that $\rho_B(r)$ is translated and rotated in six possible ways, (T;φ), which are shown as explicit parameters in this integral[19,20]. This principle is used by the Topo Geometrical Superposition Algorithm (TGSA)[19,20], which is the program used in this study to calculate the Carbó indexes via Eq. (2).

Density functional calculations were performed using the ADF code[21] employing triple-ξ Slater basis sets plus polarization functions (STO-TZP) in conjunction with the exchange expression proposed by Handy and Cohen and the correlation expression (B3LYP) considered through the generalized gradient approximation (GGA)[22]. Geometry optimizations were performed without any symmetry restrains using an analytical energy gradient method developed by Verluis and Ziegler. The magnetic response was evaluated by the NMR module of the ADF code[23].

Results and Discussion

We have taken equivalent members from each family to establish the primary differences and similarities between them, and then the predicted results are compared with those obtained experimentally.

Structural analysis of the boranes

The *closo* borane $[B_{12}H_{12}]^{2-}$ is an electron deficient cluster with an icosahedral symmetry, which is why the distances between the boron nuclei do not change appreciably in the structure. At 1.786 Å, this distance is in very good agreement with the experimental value of 1.770 Å, demonstrating the utility of our approach[25]. It is known that chemical shifts are very sensitive to geometrical changes; therefore, the quality of the results depends primarily on the quality of the obtained geometries.

The *nest* derivative of *closo*-$[B_{12}H_{12}]^{2-}$ is $B_{11}H_{15}$. The main difference between these two structures is the opening of the cage at one of its corners, with concomitant changes in the distances and chemical environments in this region of the cluster. The B-B bond distances have decreased from a maximum value of 2.041 Å to a minimum B-B distance of 1.740 Å. To the extent we move away from the opening area, both structures retain their similarities. Another variation of *nest*-$B_{11}H_{15}$ is *arachno*-$B_{10}H_{16}$, which is much less symmetrical than either the *closo* or *nest* structure. Table 1 shows that the B-B bond distances range from 2.006 Å and 1.741 Å.

Additionally, the appearance of a new type of link is observed as B-H-B. These appear in the cluster at the opening and generate tension between the B cores, giving rise to the range of the aforementioned bond distances (Table 1). This scenario leads to the 3c-2e rule of Lipscomb. The *closo* system $[B_6H_6]^{2-}$ is simply half the icosahedral closo-$[B_{12}H_{12}]^{2-}$, even though its geometry is octahedral. As in the previous structure, the B-B bond distance is 1.737, with a terminal B-H bond distance of 1.214 Å. The corresponding experimental values are 1.730 Å and 1.090 Å for the B-B bond distance and the B-H terminal bond distance in $[B_6H_6]^{2-}$, respectively[24]. Clearly, the predicted values are consistent with the experimental results. Variations in the bond distances introduce changes in the electronic environments of the boron nuclei and consequently have a direct impact on the chemical shifts. The open-caged *nest*-B_5H_9 borane exhibits C_{4V} symmetry and B-B bond distances of 1.799 Å and 1.694 Å where the cage opens, which are clearly greater than those in *closo*-$[B_6H_6]^{2-}$. By comparison, the bond distances are smaller at the bottom of the structure, which remains closed.

The borane structures studied herein are presented in Fig. 1. The main conclusion that can be drawn is that geometrical variations of the different families of borane compounds studied first involve a reduction in symmetry. This reduction increases the number of electronic environments associated with the distinct signals in the NMR spectra. Secondly, although the symmetry is reduced, the dissimilar borane structures facilitate interpretation of the chemical shifts of a given structural group, as discussed below.

In this study, we describe a detailed analysis of the chemical shifts of the investigated borane systems. The objective was to identify similarities and differences associated with the electronic environments of systems with a different number of cores. Table 2 shows the chemical shifts of various types of boron atoms with respect to B_2H_6 as the reference standard.

The chemical shifts of B and H in *closo*-$[B_{12}H_{12}]^{2-}$ are -17.58 and 1.18 ppm, respectively. These values are in good agreement with the experimental results[2], as seen in Table 2. Clearly, *closo*-$[B_{12}H_{12}]^{2-}$ possesses a unique chemical environment due to its high symmetry. On the basis of previous work[2], it is known that the chemical shifts of boron are between 0 and 50 ppm; thus, the line between high and low field is approximately 25 ppm (considering the average chemical shifts of all borane systems studied).

Table 1 – The calculated B-B bond distances (Å) in *closo*-$[B_{12}H_{12}]^{2-}$, *nest*-$B_{11}H_{15}$, and *arachno*-$B_{10}H_{16}$ borane structures[a]

closo-$[B_{12}H_{12}]^{2-}$	*nido*-$B_{11}H_{15}$	*arachno*-$B_{10}H_{16}$
B–B (1.786)	B_3–B_5 (2.040)	B_1–B_3 (1.741)
B–H terminal (1.201)	B_1–B_2 (1.880)	B_1–B_2 (1.831)
	B_1–B_9 (1.784)	B_3–B_5 (1.785)
	B_1–B_4 (1.891)	B_1–B_{10} (1.760)
	B_1–B_8 (1.910)	B_5–B_6 (1.954)
	B–H (1.299)	B_4–B_2 (1.807)
	B-H (1.357)	B6-B7 (1.855)
	B-H term (1.181)	B3-B10 (2.006)
		B-H (1.306)
		B-H (1.316)
		B-H term (1.189)

[a]Cartesian coordinates are given as supplementary data.

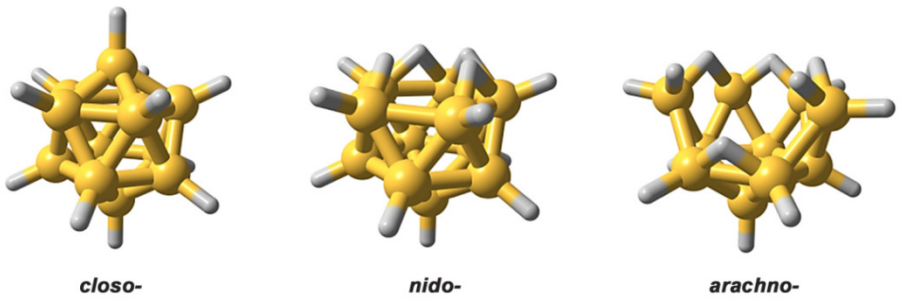

Fig. 1 — Structures of representative borane cages.

Table 2 – Theoretical and experimental chemical shifts of *closo*-, *nido*-, and *arachno*-boranes

Boron	Boron type	(σ_{dia} +	σ_{para})	σ	δ (ppm)		Difference
					Calc.	Expt.[a]	
$[B_{12}H_{12}]^{2-}$	B	187.75	-70.71	117	-17.58	-15.63	-1.95
$B_{11}H_{15}$	B1	189.67	-52.98	136.69	-30.30	-32.14	1.84
	B2	188.51	-97.92	90.58	-8.25	-9.36	1.11
	B3	190.47	-67.95	122.51	-0.29	-0.35	0.06
	B4	189.72	-70.07	119.64	-42.05	-36.87	-5.18
	B5	188.77	-82.51	106.27	-27.27	-11.22	-16.05
	B6	187.79	-71.48	116.31	-17.17	-17.4	0.23
	B7	189.18	-108.33	80.84	21.88	11.27	10.61
$B_{10}H_{16}$	B1	188.79	-99.74	89.10	10.31	-9.01	1.3
	B3	186.35	-52.78	92.15	7.26	-8.09	0.83
	B4	189.75	-63.20	133.48	-34.07	-36.32	2.55
	B6	189.73	-63.17	126.55	-27.14	-23.10	-4.04
	B10	182.57	-38.19	144.30	-44.89	-42.26	-2.63

[a]Experimental data are from Ref. 2.

Notably, the value of -17.58 ppm for *closo*-$[B_{12}H_{12}]^{2-}$ is relatively close to this midpoint, but continues to be in the high-field area.

Unlike *closo*-B_{12}, *nest*-$B_{11}H_{15}$ is missing an apex and is consequently open at one end, giving rise to three types of boron environments: B-H-B, B-B-B, and terminal B-H. Most of the chemical shift values are in the low-field region under -25 ppm, except the values -0.29 and -8.25 ppm. Additionally, the shift at -17.17 ppm found in the high-field region corresponds to a more shielded boron nuclei. The presence of these three chemical environments can justify this chemical shift behavior. In general, electron density is higher in areas with the highest number of boron atoms, and shielding of these nuclei will be higher. Furthermore, the chemical shifts of boron atoms attached to shielded hydrogen are smaller because of the lower electron density in that vicinity. Applying this criterion to *arachno*-$B_{10}H_{16}$, in which five types of boron are now possible, three different chemical environments are apparent that give rise to the range of the observed chemical shifts. The symmetry of *nest*-$B_{11}H_{15}$ is C_s; therefore, the mirror plane in the molecule causes approximately half of the boron nuclei to be identical to the other half. As seen in the chemical shift data of this borane in Table 2, seven different types of boron cores are evident.

Molecular quantum similarity (MQS) analysis

Quantum similarity using arachno-complexes

The quantum similarity indices of all complexes are shown in Tables 3–8. Table 3 gives the overlap indices of the *arachno*-complexes using Eq. 2. As seen herein, the highest value is obtained in the comparison between the complexes B_4H_{10} and B_5H_{11} (0.8345), with an Euclidean distance of 0.8173 (see also Supplementary Data, Table S1). The lowest value is between the complexes B_4H_{10} and B_9H_{15} (0.5079), with a Euclidean distance of 1.6483. Other notable higher values involve the complexes, B_8H_{14} and B_9H_{15} (0.811), with a Euclidean distance of 1.1141; $B_{10}H_{16}$ and B_9H_{15} (0.7978), with a Euclidean distance of 1.2066; and B_7H_{13} and B_8H_{14} (0.7657), with a Euclidean distance of 1.1751.

The quantum similarity using the coulomb operator, which is related to electronic properties, is also given in Table 3. The highest value is obtained between B_7H_{13} and B_8H_{14} (0.9848), with a Euclidean distance of 3.3612 (Supplementary Data, Table S2), whereas the lowest value is obtained between B_5H_{11} and B_6H_{12} (0.9210), with a Euclidean distance of 5.6048. Other high values include: B_4H_{10} and B_5H_{11} (0.9809), with a Euclidean distance of 2.9166; B_8H_{14} and B_9H_{15} (0.9803), with a Euclidean distance of 4.1360; and B_7H_{13} and B_9H_{15} (0.9799), with a Euclidean distance of 4.9324. Note that a large Euclidean distance indicates low similarity.

Quantum similarity using the closo-complexes

Table 4 shows the overlap quantum similarity values for the *closo*-complexes. In general, this overlap index is related to structural features. As seen, the highest overlap similarity value occurs between the complexes $B_{10}H_{10}$ and $B_{11}H_{11}$ (0.9114), with a Euclidean distance of 0.7680. The lowest value occurs for $B_{12}H_{12}$ and B_6H_6 (0.6732), with a Euclidean distance of 1.4432 (Supplementary Data, Table S3). In addition, high similarity values exist between the

Table 3 – MQS indices of *arachno*-complexes using the overlap operator and coulomb operator in Eq. (2)

	$B_{10}H_{16}$	B_4H_{10}	B_5H_{11}	B_6H_{12}	B_7H_{13}	B_8H_{14}	B_9H_{15}
MQS indices using overlap operator (O_I_{AB}*)*							
$B_{10}H_{16}$	1.0000						
B_4H_{10}	0.6144	1.0000					
B_5H_{11}	0.7050	0.8345	1.0000				
B_6H_{12}	0.6059	0.6624	0.5984	1.0000			
B_7H_{13}	0.6357	0.6403	0.6596	0.5551	1.0000		
B_8H_{14}	0.7376	0.6123	0.7360	0.6495	0.7657	1.0000	
B_9H_{15}	0.7978	0.5079	0.7091	0.6522	0.7524	0.8110	1.0000
MQS indices using coulomb operator (C_I_{AB}*)*							
$B_{10}H_{16}$	1.0000						
B_4H_{10}	0.9341	1.0000					
B_5H_{11}	0.9514	0.9809	1.0000				
B_6H_{12}	0.9331	0.9281	0.9210	1.0000			
B_7H_{13}	0.9616	0.9605	0.9636	0.9350	1.0000		
B_8H_{14}	0.9724	0.9435	0.9489	0.9349	0.9848	1.0000	
B_9H_{15}	0.9796	0.9288	0.9571	0.9507	0.9799	0.9803	1.0000

Table 4 – MQS indices of *closo*-complexes using the overlap operator and coulomb operator in Eq. (2)

	$B_{10}H_{10}$	$B_{11}H_{11}$	$B_{12}H_{12}$	B_5H_5	B_6H_6	B_7H_7	B_8H_8	B_9H_9
MQS indices using overlap operator (O_I_{AB}*)*								
$B_{10}H_{10}$	1.0000							
$B_{11}H_{11}$	0.9114	1.0000						
$B_{12}H_{12}$	0.8039	0.9139	1.0000					
B_5H_5	0.6817	0.5088	0.4820	1.0000				
B_6H_6	0.7219	0.6962	0.6732	0.7807	1.0000			
B_7H_7	0.7756	0.7491	0.7096	0.7828	0.8181	1.0000		
B_8H_8	0.8358	0.7831	0.7574	0.7351	0.8032	0.8909	1.0000	
B_9H_9	0.9031	0.8362	0.7873	0.7170	0.7497	0.7909	0.8510	1.0000
MQS indices using coulomb operator (C_I_{AB}*)*								
$B_{10}H_{10}$	1.0000							
$B_{11}H_{11}$	0.9941	1.0000						
$B_{12}H_{12}$	0.9875	0.9939	1.0000					
B_5H_5	0.9470	0.8965	0.8828	1.0000				
B_6H_6	0.9702	0.9612	0.9529	0.9775	1.0000			
B_7H_7	0.9770	0.9650	0.9623	0.9754	0.9853	1.0000		
B_8H_8	0.9860	0.9793	0.9788	0.9650	0.9809	0.9909	1.0000	
B_9H_9	0.9928	0.9880	0.9856	0.9565	0.9711	0.9845	0.9911	1.0000

complexes $B_{11}H_{11}$ and $B_{12}H_{12}$ (0.9139), with a Euclidean distance of 0.7951, and $B_{10}H_{10}$ and B_9H_9 (0.9031), with a Euclidean distance of 0.7639.

As seen from the coulomb similarity for this family of complexes, the highest value of 0.9941 occurs between $B_{10}H_{10}$ and $B_{11}H_{11}$ (Table 4), with a Euclidean distance of 2.6670 (Supplementary Data, Table S4). The lowest value corresponds to $B_{12}H_{12}$ and B_5H_5 (0.8828), with a Euclidean distance of 13.9897. Clearly, this family of borane complexes has high values of electronic similarity, which are generally above 0.9000.

Quantum similarity using nido-complexes

Table 5 shows the overlap similarity of various *nido*-complexes. As seen, the highest value is observed in the comparison of $B_{10}H_{14}$ and B_4H_8 (0.5114), with a Euclidean distance of 1.6557 (Supplementary Data, Table S5). The lowest value occurs for B_6H_{10} and B_7H_{11} (0.9055), with a Euclidean distance of 0.6829. The lowest values are obtained using the overlap similarity with respect to the *arachno*- and *closo*-complexes.

To evaluate the electronic similarity, the coulomb similarity was also calculated (Table 5). The highest value is determined for $B_{10}H_{14}$ and $B_{11}H_{15}$ (0.9917), with a Euclidean distance of 3.2553 (see Supplementary Data, Table S6). The lowest value occurs for the comparison between B_4H_8 and B_8H_{12} (0.9214), with a Euclidean distance of 8.5514. In general, this family of complexes possesses high values of electronic similarity.

Table 5 – MQS indices of *nido*-complexes using the overlap operator and coulomb operator in Eq. (2)

O_I_{AB}	$B_{10}H_{14}$	$B_{11}H_{15}$	B_4H_8	B_5H_9	B_6H_{10}	B_7H_{11}	B_8H_{12}	B_9H_{13}
MQS indices using overlap operator (O_I_{AB})								
$B_{10}H_{14}$	1.0000							
$B_{11}H_{15}$	0.8611	1.0000						
B_4H_8	0.5114	0.5198	1.0000					
B_5H_9	0.6541	0.6467	0.7555	1.0000				
B_6H_{10}	0.7589	0.7481	0.6171	0.8123	1.0000			
B_7H_{11}	0.7309	0.7649	0.5881	0.7304	0.9055	1.0000		
B_8H_{12}	0.8625	0.8135	0.5915	0.6985	0.8181	0.8948	1.0000	
B_9H_{13}	0.7257	0.7180	0.5643	0.7341	0.5491	0.6140	0.7012	1.0000
MQS indices using coulomb operator (C_I_{AB})								
$B_{10}H_{14}$	1.0000							
$B_{11}H_{15}$	0.9917	1.0000						
B_4H_8	0.9129	0.9128	1.0000					
B_5H_9	0.9558	0.9478	0.9761	1.0000				
B_6H_{10}	0.9468	0.9540	0.9515	0.9840	1.0000			
B_7H_{11}	0.9582	0.9733	0.9471	0.9699	0.9893	1.0000		
B_8H_{12}	0.9823	0.9753	0.9214	0.9604	0.9762	0.9919	1.0000	
B_9H_{13}	0.9785	0.9780	0.8959	0.9313	0.8917	0.9535	0.9522	1.0000

Conclusions

The computational tools employed herein have proven useful in describing the structural properties of three families of borane systems (i.e., *closo*, *nest*, and *arachno*) examined in this study, as evidenced by the good correlation between the calculated values determined herein and previously reported experimental values. Three types of environments were identified for the borane systems, in increasing order of chemical shielding as: B-H < B-H-B < B-B-B. These results allowed us to interpret the chemical shifts for a wide range of borane systems. The obtained chemical shifts are in good agreement with the available experimental results and reflect the extent of heterogeneity of the electronic environments present in these chemical systems in terms of symmetry and the number of boron cores. The results presented herein were supported by molecular quantum similarity studies using similarity descriptors (e.g., overlap and coulomb indices and their Euclidean distances). Quantum similarity can be related to the electronic structures in each family of borane complexes and therefore has wide scope for describing many other types of systems. It is recommended that the level of theory used in this work be used in future studies to describe boranes cages derived from heteroboranes, boranes, carboranes, and haloboranes. Future studies will include determining the electronic and structural properties of large polyhedral comprising the merger between various boranes and derivatives, including fusion boranes with *closo*, *nest*, and/or *arachno*-type features. Analogous cluster systems such as those involving Al (e.g. *closo*-$Al_{12}H_{14}$) have gained increased attention recently and will also be investigated.

Supplementary Data

Supplementary data associated with this article are available in the electronic form at http://www.niscair.res.in/jinfo/ijca/IJCA_57A(02)143-149_SupplData.pdf.

Acknowledgement

Financial assistance from the Universidad de Talca, Santiago, Chile (Projects nos FONDECYT 3150035 and 1130007) is gratefully acknowledged.

References

1 Cavanaugh M, Fehlner T P, Stramel R, O'Neill M E & Wade K, *Polyhedron*, 4, (1985) 687.
2 Hermanek S, *Chem Rev*, 92 (1992) 325.
3 Grimes R N, In *Structures and Mechanisms*, Vol. 827 (ACS Symposium Series), 2002, Chap. 2, p. 20.
4 Chen Z & King R B, *Chem Rev*, 105 (2005) 3613.
5 Jemmis E D & Prasad D L V K, *J Solid State Chem*, 179 (2006) 2768.
6 Lipscomb W N, *J Less Common Met*, 82 (1981) 1.
7 Spielman J R, *Synth React Inorg Met Chem*, 6 (1975 319.
8 Van N, Tiritiris I, Winter R F, Sarkar B, Singh P, Duboc C, Muñoz-Castro A, Arratia-Pérez R, Kaim W & Schleid T, *Chemistry*, 16 (2010) 11242.
9 (a) *Nuclear Magnetic Shielding and Molecular Structure*, edited by J A Tossell, NATO ASI Series Vol. C 386 (Kluwer, Dordrecht) 1993; (b) Kaupp M & Malkin V G, Eds. *J Comput Chem*, 20 (1999) 1199.

10 Bazargani M & Tafazzoli M, *APCBEE Procedia*, 7 (2013) 151.
11 Muñoz-Castro A, *Chem Phys Lett*, 555 (2013) 282.
12 Carbó-Dorca R, Arnau M & Leyda L, *Int J Quant Chem*, 17 (1980) 1185.
13 Amat L & Carbó-Dorca R, *Int J Quant Chem*, 87 (2002) 59.
14 Gironés X & Carbó-Dorca R, *QSAR Comb Sci*, 25 (2006) 579.
15 Carbó-Dorca R & Gironés X, *Int J Quant Chem*, 101 (2005) 8.
16 (a) Morales-Bayuelo A, Torres J & Vivas-Reyes R, *Int J Quant Chem*, 112 (2012) 2637; (b) Morales-Bayuelo A & Vivas-Reyes R, *J Math Chem*, 51 (2013) 1835; (c) Morales-Bayuelo A, *Int J Quant Chem*, 113 (2013) 1534; (d) Morales-Bayuelo A, Baldiris R & Vivas-Reyes R, *J Theoret Chem*, 13 (2013) 1; (e) Morales-Bayuelo A, *J Mol Mod*, 22 (2016) 164; (f) Morales-Bayuelo A, *Molecules*, 22 (2017) 1027.
17 Morales-Bayuelo A & Vivas-Reyes R, *J Math Chem*, 51 (2013) 125.
18 Morales-Bayuelo A, Torres J, Baldiris R & Vivas-Reyes R, *Int J Quant Chem*, 112 (2012) 2681.
19 Morales-Bayuelo A, Torres J & Vivas-Reyes R, *J Theoret Comp Chem*, 11 (2012) 223.
20 Gironés X, Robert D & Carbó-Dorca R, *J Comput Chem*, 22 (2001) 255.
21 Joseph J, Gimarct M & Zhao M, *Polyhedron*, 12 (1993) 2841.
22 Te Velde G T, Bickelhaupt F M, Baerends E J, Fonseca Guerra C, van Gisbergen S J, Snijders J G & Ziegler T, *J Comput Chem*, 22 (2001) 931.
23 Perdew J P, Chevary J A, Vosko S, Jackson K A, Pederson M R, Singh D & Fiolhais C, *Phys Rev B*, 46 (1992) 6671.
24 Hwang S J, Bowman R C, Reiter J W, Rijssenbeek J, Soloveichik G L, Zhao J C, Kabbour H & Ahn C C, *J Phys Chem C*, 112 (2008) 3164.